JOURNAL OF GEOPHYSICAL RESEARCH, VOL. 113, B09207, doi:10.1029/2007JB005555, 2008

In situ production of ash in pyroclastic flows

J. Dufek[1,2] and M. Manga[1]

Received 17 December 2007; revised 28 April 2008; accepted 23 June 2008; published 16 September 2008.

[1] Abrasion and comminution of pumice clasts during the propagation of pyroclastic flows have long been recognized as a potential source for the enhanced production of volcanic ash, however, their relative importance has eluded quantification. The amount of ash produced in situ can potentially affect runout distance, deposit sorting, the volume of ash introduced in the upper atmosphere, and internal pore pressure. We conduct a series of laboratory experiments on the collisional and frictional production of ash that may occur during different regimes of pyroclastic flow transport. Ash produced in these experiments is predominately 10–100 microns in size and has similar morphology to tephra fall ash from Plinian events. We find that collisional ash production rates are proportional to the square of impact velocity. Frictional ash production rates are a linear function of the velocity of the basal, particle-enriched bed load region of these flows. Using these laboratory experiments we develop a subgrid model for ash production that can be included in analytical and multiphase numerical procedures to estimate the total volume of ash produced during transport. We find that for most flow conditions, 10–20% of the initial clasts comminute into ash with the percentage increasing as a function of initial flow energy. Most of the ash is produced in the high-energy regions near the flow inlet, although flow acceleration on steep slopes can produce ash far from the vent. On level terrain, collisionally and frictionally produced ash generates gravity currents that detach from the main flow and can more than double the effective runout distance of these flows. Ash produced at the frictional base of the flow and in the collisional upper regions of the flow can be redistributed through the entirety of the flow, although frictionally produced ash accumulates preferentially near its source in the bed load. Flows that descend steep slopes produce the majority of their ash in the collisonally dominant flow head and flow snouts likely develop subangular to rounded pumice during this process.

Citation: Dufek, J., and M. Manga (2008), In situ production of ash in pyroclastic flows, *J. Geophys. Res.*, *113*, B09207, doi:10.1029/2007JB005555.

1. Introduction

[2] Ground-hugging pyroclastic density currents are commonly generated by explosive volcanic eruptions, and encompass a range of particle concentrations and particle sizes inherited from the initial fragmentation event and modified during subsequent transport [*Wohletz et al.*, 1989]. The largest of these density currents produce massive ignimbrites and are the most voluminous single ash sources to the atmosphere, having potentially dramatic effects on climate [*Perkins and Nash*, 2002; *Self*, 2006; *Sparks and Wilson*, 1976; *Valentine and Wohletz*, 1989; *Walker*, 1981; *Wilson and Hildreth*, 1997]. More common, and smaller volume, pyroclastic density currents are an immediate hazard to surrounding population centers, and the associated ash can induce long-term respiratory problems [*Calder et al.*, 1999; *Cole et al.*, 2002; *Edmonds et al.*, 2006; *Fisher et al.*, 1987; *Horwell and Baxter*, 2006]. These flows are also agents of rapid landscape evolution near steep volcanic edifices.

[3] Most field interpretations and models of pyroclastic density currents are based on the premise that the fraction of ash (particle sizes less than 2 mm) in an eruption is determined by the initial fragmentation of the magma in the volcanic conduit. Understanding of conduit fragmentation has made several advances in the past decade [*Dingwell*, 1996; *Gardner et al.*, 1996; *Gonnermann and Manga*, 2003; *Papale*, 1999; *Zhang*, 1999; *Zimanowski et al.*, 2003]. However, abrasion and comminution during transport have long been recognized as a potential source for the enhanced production of volcanic ash, although quantification has proved elusive [*Schwarzkopf et al.*, 2007; *Walker*, 1981]. Previous experiments on the phenomena are sparse. Impact experiments of basaltic andesite particles showed significant breakage upon impact [*Schwarzkopf et al.*, 2007] and this process may operate across a range of compositions and flow concentrations.

[4] The rounding of pumice commonly observed in many pyroclastic density current deposits also indicates in situ

[1]Department of Earth and Planetary Science, University of California Berkeley, Berkeley, California, USA.
[2]Now at School of Earth and Atmospheric Sciences, Georgia Institute of Technology, Atlanta, Georgia, USA.

0148-0227/08/2007JB005555$09.00

Figure 1. Pyroclastic flow deposit from Mount St. Helens in 1980 showing some rounding of pumice clasts. USGS photograph.

particle-particle collisions and abrasion. Pumice particles immediately following fragmentation in the conduit are often angular as demonstrated by tephra fall deposits and experiments [*Spieler et al.*, 2003]. *Spieler et al.* [2003] initiated fragmentation in laboratory experiments for Mount St. Helens dacite over a range of temperature and pressure changes; in all cases, the fragments are angular. However, pumice in deposits from small volume pyroclastic density currents from Mount St. Helens (with nearly identical chemical composition) are visibly rounded (Figure 1). The rounding of particles can represent a considerable loss of the volume fraction of the initial particle; for instance, the reduction of a cube to sphere of the same diameter is approximately a ~48% volume reduction. Rounding of clasts has been observed for a variety of compositions (andesite – rhyolite) and eruption styles (e.g., vulcanian, column collapse, dome collapse) [*Allen*, 2001; *Calder et al.*, 1999, 2000].

[5] Further evidence for abrasion and comminution comes from crystal-scale measurements. *Freundt and Schmincke* [1992] used glass adhering to crystals in non-welded Laacher See pyroclastic flow deposits as a measure of abrasion during transport. They showed that the sanidine crystals from flow deposits had significantly smaller glass rims than crystals from tephra fall deposits. No systematic variation in glass rim thickness was observed at different radial distances from the vent leading these authors to conclude that the majority of abrasion occurred in the near-vent, column collapse region. Sanidine crystals are themselves more abraded in pyroclastic flow deposits in the Latera Volcanic Complex relative to fall counterparts [*Taddeucci and Palladino*, 2002]. An added complication is that particle collisions within the volcanic conduit may also cause further particle breakup [*Dufek and Bergantz*, 2005; *Kaminski and Jaupart*, 1998] apart from abrasion during pyroclastic flow transport, which may explain the qualitative lack of difference in glass adhering to crystals from Crater Lake fall and flow deposits [*Fisher*, 1963]. Regardless, the conditions for in situ ash production and the relative volume of comminuted ash in flows remain poorly constrained.

[6] The amount of ash produced in situ can potentially affect runout distance, internal pore pressure in the flow, deposit sorting, and the volume of ash introduced in to the upper atmosphere. Generation of finer particles enhances the number of particles in the suspended load region of the flow, where turbulence and particle-particle interactions maintain fine particles in a suspension. Suspended load currents can detach from the basal, particle dense layer, surmount topography, and travel further than some confined dense flows [*Calder et al.*, 1999; *Dufek and Bergantz*, 2007b; *Miller and Smith*, 1977]. Scaling analyses indicate that both velocity and runout distance should increase as the mass of fine particles increases in the suspended load [*Britter and Simpson*, 1978; *Bursik and Woods*, 1996; *Dade and Huppert*, 1995; *Simpson*, 1997].

[7] Here we quantify the production of in situ ash during the transport of pyroclastic density currents using a combined experimental, theoretical and computational approach. In section 2, we describe a series of laboratory experiments on the collisional production of ash during different regimes of pyroclastic flow transport. Using these laboratory experiments we develop a subgrid model for ash production that can be included in analytical and multiphase numerical approaches to estimate the total volume of ash produced during transport (section 3 and 4). In section 5 we combine ash production measurements and an analytical model to assess the relative importance of ash production in the suspended load relative to the bed load regions on level

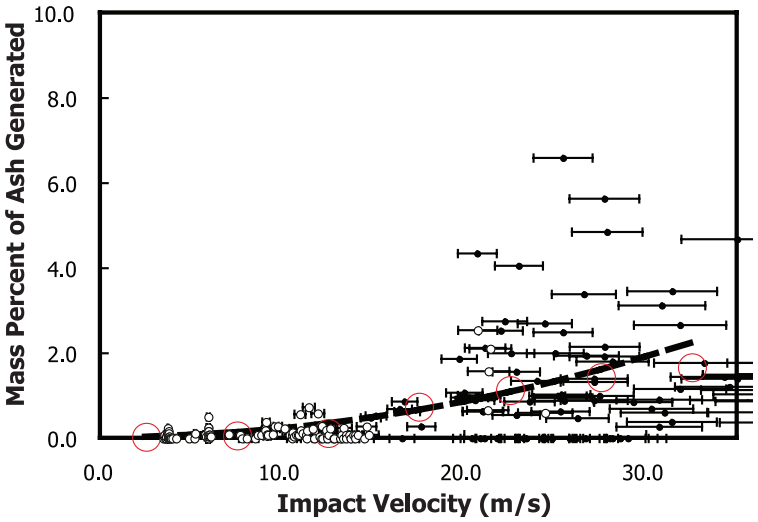

Figure 2. Mass percent of ash produced as a function of particle impact velocity during particle-particle collisions. This compilation contains experiments with unmachined (natural, angular) pumice particles, shown with open circles, and machined pumice particles shown as black circles [*Cagnoli and Manga*, 2003]. Error in the mass percent of ash generated is smaller than the symbols. Impact velocity error bars are determined from the frame rate of the high-speed video. The data were binned in 5 m/s increments to remove biases of having greater data coverage at low velocity (large red open circles). The scatter in the data reflects irregularity in the shape, density, and strength of individual pumice clasts.

terrain. We then examine numerically the effect of initial flow energy and bed slope on ash production (section 6).

2. Experimental Comminution

[8] We conducted laboratory experiments to examine the role of short-duration particle collisions on the comminution of pumice. We also analyzed the experiments of *Cagnoli and Manga* [2004] to determine the rate of ash production when particles make enduring frictional contact with other particles or the bed. In both cases, the pumice used was from tephra fall deposits of Medicine Lake Volcano in northern California, with an average density of 550 ± 39 kg/m^3 and bubble size mode smaller than 1 mm [*Cagnoli and Manga*, 2004].

[9] The pumice collision experiments were conducted with pumice particles with masses between 0.5 to 4.2 g, and impact velocities ranging from 3.45 to 35.0 m/s. Single pumice particles were either dropped from height or propelled by compressed air in a 'pumice gun' onto a pumice target [*Cagnoli and Manga*, 2003]. We included the measurements of *Cagnoli and Manga* [2003] that used pumice particles machined to form cylinders with data collected using nonmachined samples, all Medicine Lake pumice. Precollision impact velocity was measured using high-speed video taken at 2000 frames per second. Mass before and after the impact was recorded on a digital Ohaus scale with 0.001 g accuracy. All the experiments were conducted at room temperature; on the basis of the experiments of *Schwarzkopf et al.* [2007], we expect only a small dependence of particle breakup on temperature. We performed a total of 356 collision experiments and the results are compiled in Figure 2.

[10] We performed a least squares fit on the data in Figure 2 to determine an empirical relationship for the percentage of ash produced per collision. To account for the experimental error in measuring velocity, as well as to remove the bias of having more measurements at lower velocities, we bin the data in 5 m/s increments (shown as large open circles in Figure 2). The rate of collisional ash production (ψ) is given as

$$\psi(\Delta u) = N\Delta u^2, \tag{1}$$

where N = 2.1 × 10^{-5} s^2/m^2 and Δu is the impact velocity. The dependence on the square of the velocity is motivated by the distribution of the data and is consistent with ash production being related to the kinetic energy of the impacts. For the particle velocities we considered, almost all material loss for single collisions was in the form of ash size particles rather than pieces comprising 5% or greater of the mass of the impacting pumice. Other experiments using synthetic and natural materials have shown a threshold behavior; the highest energy impacts produce fractal size distributions, whereas lower energy impacts exploit weaknesses near the periphery of the particles thus creating primarily small particles [*Inaoka and Ohno*, 2003]. We surmise that the bubble walls break relatively easily and dissipate much of the collisional energy.

[11] Particles at the base of granular flows can often form bed load regions where particles make enduring frictional contact with the bed and each other. *Cagnoli and Manga* [2004] performed a series of experiments in a shear cell, where rotation of a rough disk generated motion in the granular flow with approximately 0.4 volume fraction particles. These experiments were again performed with natural Medicine Lake pumice. They found a linear rate of ash production as a function of flow velocity. The rate of production as a function of linear velocity is given by

$$\xi(u) = Mu, \tag{2}$$

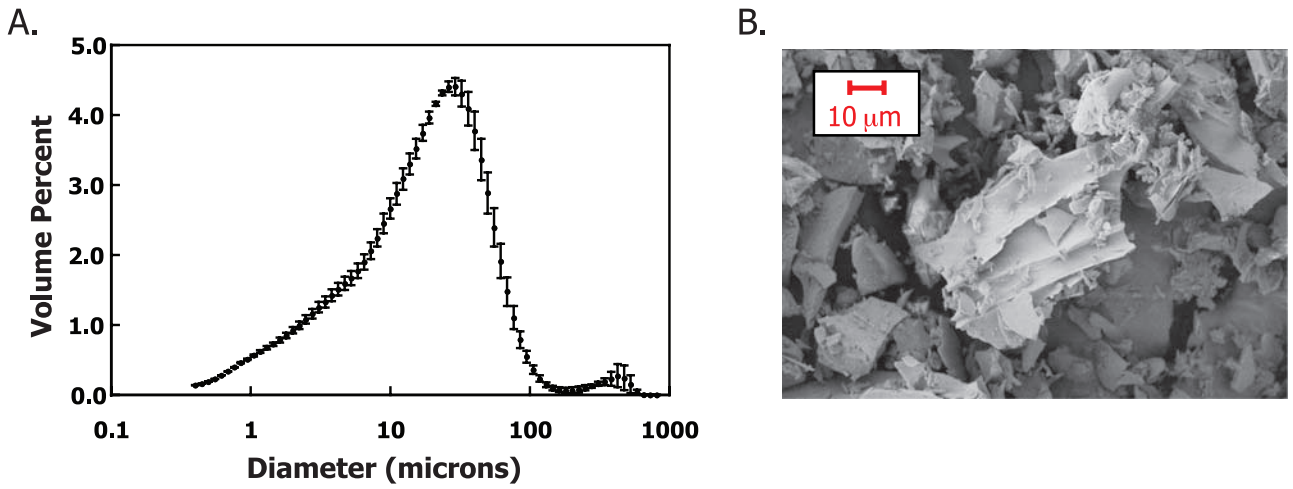

Figure 3. (a) Size distribution of the frictionally produced ash. Size distribution determined by a Coulter LS 100 laser diffraction size distribution analyzer. (b) SEM image of ash produced by frictional interaction. Ash morphology is similar to plinian ash (angular, curved shards from bubble walls) [*Heiken and Wohletz*, 1985].

where M = 0.0045 kg/m^3. The particles produced in this experiment were analyzed using a Coulter LS 100 laser diffraction analyzer to determine the size distribution (Figure 3) with the majority of fines in the range of 10–100 microns.

3. Conversion to Rate Expression for Continuum Methods

[12] In the theoretical analysis and computational approach presented later we need to know the mass of ash generated per volume. From the shear cell experiments we estimate that the majority of shear is accommodated near the base of the flow, typically within five particle diameters of the base. The rate of production of frictionally produced ash, R_{24}, is then given as

$$R_{24} = \frac{1}{\Delta y}\xi(u), \tag{3}$$

where Δy is the height above the bed where the majority of ash is produced. The subscript 2 refers to large pumice particles, the subscript 3 refers to ash produced by collisions, and the subscript 4 refers to ash produced by bed friction. We will use the term pumice to generically refer to the large particles in the flow and ash to refer to the fine component.

[13] The collisional production of ash from the experiments is given on a per collision basis, and requires further analysis to recast it into a form suitable for continuum mechanics. We use kinetic theory to incorporate the single collision measurements into a continuum rate of production on the basis of the total number of expected particle encounters. This rate, R_{23}, is given as

$$R_{23} = \underbrace{\frac{144(\alpha_2)^2\sqrt{\theta}g_0}{\pi^{3/2}(d_2)^4}}_{\text{Collision Frequency}} \times \underbrace{\psi(\Delta\bar{u})}_{\substack{\text{Mass Fraction}\\ \text{of ash per}\\ \text{collision}}} \times \underbrace{\frac{\rho_2\pi(d_2)^3}{6}}_{\text{Mass per particle}}. \tag{4}$$

The collision frequency is derived by integrating the joint probability distributions for two particles [*Chapman and Cowling*, 1952; *Gidaspow*, 1994]. Here α_2 is the particle volume fraction, θ is the granular temperature, or fluctuating component of the particle velocity field, d_2 is the particle diameter, and $\Delta\bar{u}$ is the average impact velocity. The radial distribution function, g_0, is given by

$$g_0 = \left[1 - \left(\frac{\alpha_2}{\alpha^{CP}}\right)^{1/3}\right]^{-1}. \tag{5}$$

Here the close packing volume fraction (~0.6) is given by α^{CP}. Intuitively, as the particle volume fraction increases the collisional frequency increases. The collisional frequency asymptotes to infinity at close packing where particles are in constant contact. However, the relation given in equation (4) is not valid at close packing as it applies to discrete, binary collisions and we bound its use in the following approaches to volume fractions less than the close packing volume fraction of particles.

[14] To determine the average impact velocity ($\Delta\bar{u}$), we first determine the probability distribution for impact velocity, and then integrate over all possibilities to determine the average impact velocity. Details of this analysis are given in Appendix A.

[15] After integrating over the collisional probability distribution, we obtain the average impact velocity

$$\Delta\bar{u} = \sqrt{\theta/\pi}. \tag{6}$$

Using equation (1) for ash produced per collision, the production rate becomes

$$R_{23} = \frac{24(\alpha_2)^2\theta^{3/2}N(\rho_2)g_0}{\pi^{3/2}(d_2)}. \tag{7}$$

4. End-Member Transport Models: An Analytical Examination

[16] We now present a simplified analytical transport model that incorporates the experimentally derived ash

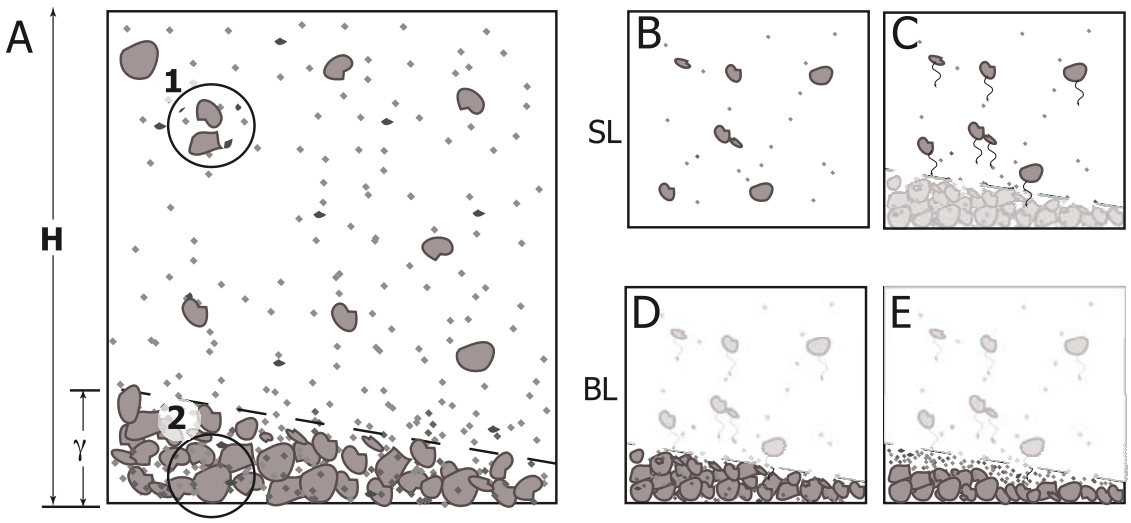

Figure 4. Schematic illustration of ash production end-member processes. (a) The analytical calculations are split between suspended load (circle 1) that consists of collisionally produced ash, and bed load (circle 2) that consists of frictionally produced ash. Two sets of assumptions bracket the analytical suspended load and bed load models. In the suspended load (SL), the two assumptions are (b) no particle settling and (c) particle settling based on the settling velocity of a single particle in still air. The bracketing assumptions for bed load (BL) are (d) well mixed (pumice and ash particles) within the bed load and (e) segregated bed load where all large particles settle to the base of the flow. In the diagram, H denotes the total flow thickness and γ denotes the bed load thickness.

production rates in order to obtain insight into the relative importance of ash production under end-member flow conditions. For these analytical models we conceptually split the flow into two different ash-producing zones as depicted in Figure 4: first, a suspended load region where the particle concentration is low and collisions dominate ash production, and second a bed load region where frictional interactions at the base of the flow produces the ash. We consider a flow that is initially composed entirely of suspended load material of height H. The bed load region forms as particles settle from the suspended load into the bed load.

[17] Ash produced in the suspended load and bed load are analyzed separately, where once again the subscript 2 refers to the large particles initially present in a flow, the subscript 3 refers to ash produced in the suspended load and the subscript 4 refers ash produced in the bed load. For both the suspended load and bed load cases, two end-member conditions are examined that bound the amount of ash produced in these settings. In these calculations and in the following computational models the large particles, or pumice, initially present are assumed to have a diameter of 1.0 cm and density of 500 kg/m^3. The ash particles produced during transport are assumed to have a diameter of 100 microns and a density of 2000 kg/m^3.

4.1. Analytical Model for Suspended Load Ash

[18] Particle removal and dilution of the suspended load region occurs as particles settle into the underlying bed load region. One end-member is to assume that the particles in the suspended load are completely supported by either particle-particle interaction or by turbulence (Figure 4b). In this case, loss of the initial volume of large particles only occurs as a result of collisional comminution. At the other extreme we assume that particle loss from the suspended load region is based on the settling velocity (Figure 4c). In this case, loss of the large particles in the suspended load is due to both settling out of particles and collisional comminution.

[19] We derive the expressions for the temporal evolution of the volume fraction of pumice and volume fraction of collisionally produced ash on the basis of the following simplifying assumptions: (1) Rate of production of granular temperature by shear is balanced by dissipation by inelastic collisions, i.e.,

$$\mu_p \left(\frac{\partial U}{\partial y}\right)^2 = \varepsilon_c, \tag{8}$$

where ε_c is the energy dissipation rate per volume (the product of the energy lost during one collision event and the number of collisions), and μ_p is the viscosity of a dilute granular flow [*Chapman and Cowling*, 1952; *Gidaspow*, 1994]. (2) The densimetric Froude number of the current is approximately $\sqrt{2}$, and sets the front speed of the current [*Britter and Simpson*, 1978; *Dade and Huppert*, 1995; *Simpson*, 1997]

$$U = \sqrt{\frac{2\alpha_p\left(\rho_p - \rho_1\right)gH}{\rho_1}}. \tag{9}$$

(3) The velocity gradient and particle concentration are vertically uniform (well mixed).

[20] We stress that we do not necessarily consider these assumptions to be realistic (in particular, the more detailed numerical analysis that follows shows that assumption 3 is in general not valid). However, these relatively straightforward analytical expressions for the end-member behavior

are useful to gauge the relative importance of different processes, and also provide a reference for interpreting numerical simulations. The detailed derivation of the following expressions is included in the Appendices B–D, and here we show some of the more salient features.

[21] In the case that no particles are lost by settling, the previous set of assumptions leads to the following temporal evolution of the volume fraction of ash particles (Figure 4b):

$$\alpha_3^S = \alpha_2 - \sqrt{\alpha_2^2 - 2Bt}, \tag{10}$$

provided

$$t < \frac{\alpha_2^S}{2B}. \tag{11}$$

Here B is a constant that depends on the initial conditions of flow

$$B = \left[\frac{24N}{\pi^{3/2} d_2}\right]\left[\frac{5\pi^2 d_2^2 \alpha_2 (\rho_2 - \rho_1) g}{144(1-e^2) H \rho_1}\right]^{3/2}, \tag{12}$$

where N is experimentally determined (equation (1)), d_2 is the diameter of the pumice particles, e is the restitution coefficient, and ρ_1 and ρ_2 are densities of gas and particle, respectively. When time equals $\alpha_2^S/2B$ all the large particles are removed from the flow by collisions.

[22] When particles are removed from the suspended load by settling, the volume fraction of large particles present in the system decays exponentially with time. This affects the collisional production of ash in two ways. First, the dilution of particle volume fraction results in a decreasing probability of particle collisions. Second, velocity (and velocity gradients) decreases as the bulk density contrast between the current and ambient air diminishes. This results in a decrease in the production of the fluctuating part of the particle velocity distribution, i.e., the granular temperature. The more coherent (small granular temperature) the flow becomes the fewer collisions take place. The volume fraction of ash in the flow for these conditions is

$$\alpha_3 = \frac{2H}{w_s \alpha_1^0} B\left(1 - \exp\left[\frac{-w_s t}{2H}\right]\right), \tag{13}$$

where w_s is the settling velocity of a single particle in a still fluid, α_1^0 is the volume fraction of large particles initially present, and B depends on the flow initial conditions (equation (12)). The final volume of comminuted ash in the suspended load is ultimately determined by the length of time pumice remains in suspension and will always be less than the complete suspension end-member.

4.2. Bed Load Production of Ash

[23] The formation of a bed load region implies some transfer of particles from the suspended load to the basal, particle-concentrated zone. As described earlier, the simplest possible assumption for this transmission of particles is that particles settle to form the bed load. Again, we make the tentative assumption that the settling of particles can be described by the single particle settling velocity. The corollary to the exponential decay in volume fraction from the suspended load is the following relationship for the thickness of the bed load region

$$\gamma = \frac{\alpha_2^0 H\left(1 - \exp\left[\frac{-w_s t}{H}\right]\right)}{\alpha^{CP} - \alpha_2^0 \exp\left[\frac{-w_s t}{H}\right]}. \tag{14}$$

This expression assumes that the bed load is at the close packing volume fraction for particles (α^{CP}) and that no particles leave the bed load (either through reentrainment by the suspended load or through permanent deposition). In our analytical model for bed load ash production, the following simplifications are used:

[24] 1. Bed load ash is produced in a thin layer, with thickness l, near the bed because of differential motion of the granular flow and the stationary bed. On the basis of the experiments we assign this layer a thickness of five particle diameters.

[25] 2. The velocity of the bed load matches the front velocity of the overlying suspended load (determined from particle concentration and the Froude number condition).

[26] This last assumption is an obvious simplification, and some of the later numerical simulations are aimed at identifying the conditions for which this assumption is violated.

[27] Two end-member conditions are examined (Figures 4d and 4e). In the first, the granular mixture is composed of pumice and the frictionally produced ash and flow is well mixed. As more ash is produced, the pumice volume fraction is diluted in the layer immediately adjacent to the ground where ash in being produced, hence reducing ash production. The volume fraction of frictional ash is then given by

$$\begin{aligned}\alpha_4 &= \alpha^{CP}\left[1 - \exp\left(\frac{-2HM}{\alpha^{CP} w_s \rho_2 l}\sqrt{\frac{2(\rho_2 - \rho_1) g H \alpha_2^0}{\rho_1}}\right)\right. \\ &\quad \left.\cdot\left(1 - \exp\left[\frac{-w_s t}{2H}\right]\right)\right] \\ &\approx \alpha^{CP}\left[1 - \exp\left(\frac{-2HM}{\alpha^{CP} w_s \rho_2 5 d_2}\sqrt{\frac{2(\rho_2 - \rho_1) g H \alpha_2^0}{\rho_1}}\right)\right. \\ &\quad \left.\cdot\left(1 - \exp\left[\frac{-w_s t}{2H}\right]\right)\right],\end{aligned} \tag{15}$$

where we assume that $l = 5d_2$.

[28] The other end-member assumes that large particles and ash particles completely segregate in the bed load region, so that the pumice particles congregate at the base of the flow (Figure 4e). The concentration is then

$$\begin{aligned}\alpha_4 &= \left(1 - \exp\left[\frac{-w_s t}{2H}\right]\right)\frac{2HM}{w_s \rho_2 l}\sqrt{\frac{2(\rho_2 - \rho_1) g H \alpha_2^0}{\rho_1}} \\ &\approx \left(1 - \exp\left[\frac{-w_s t}{2H}\right]\right)\frac{2HM}{w_s \rho_2 5 d_2}\sqrt{\frac{2(\rho_2 - \rho_1) g H \alpha_2^0}{\rho_1}}.\end{aligned} \tag{16}$$

In this case, the production of ash by friction is not limited by particle dilution in the bed load.

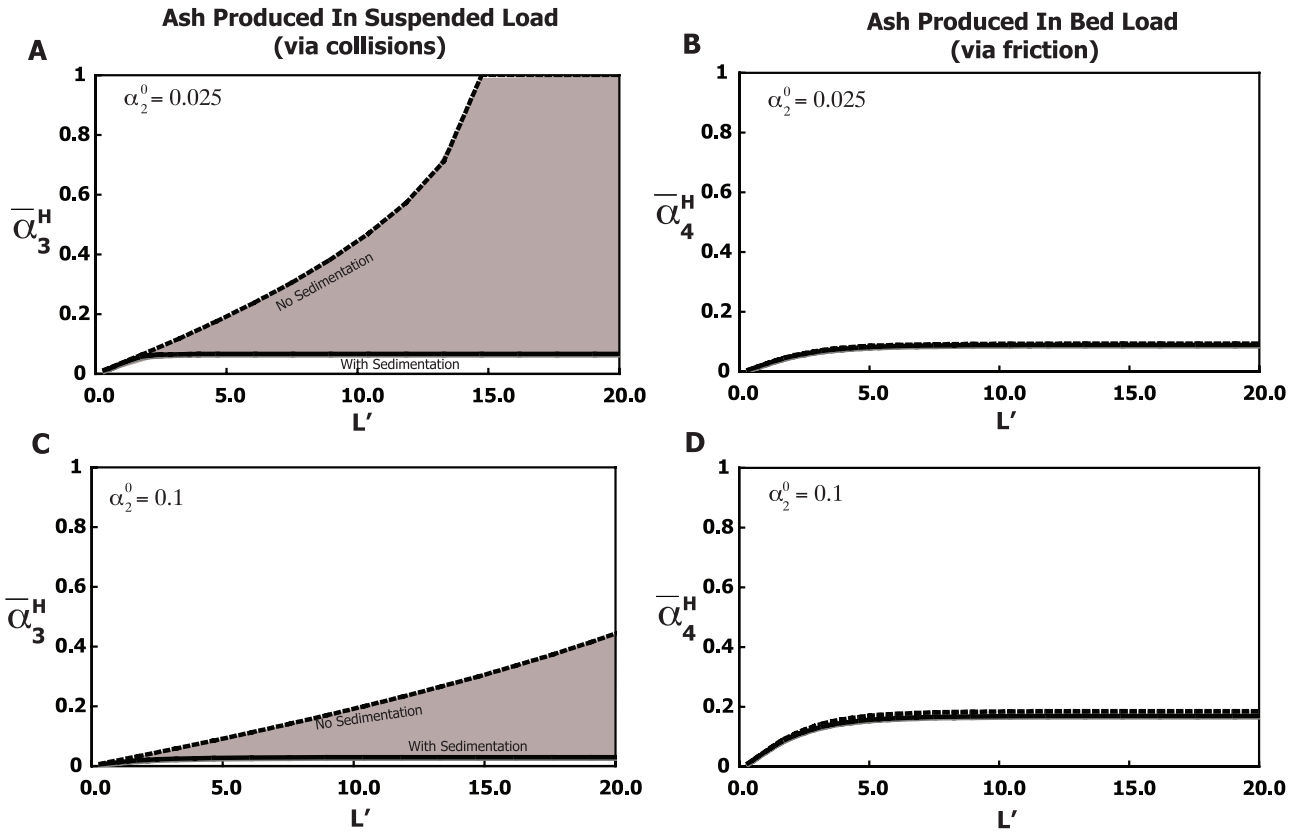

Figure 5. Analytical end-member calculations for suspended load and bed load over level terrain. In the diagram, $\overline{\alpha}_3{}^{\mathrm{H}}$ indicates the volume ratio of ash produced by collisions relative to pumice, and $\overline{\alpha}_4{}^{\mathrm{H}}$ denotes this ratio for frictionally produced ash. (a and b) The suspended load and bed load ash production for dilute ($\alpha_2{}^0 = 0.025$) conditions, respectively, and (c and d) the suspended load and bed load calculations for denser initial conditions ($\alpha_2{}^0 = 0.1$), respectively. In Figures 5a and 5c, the dashed line indicates the no sedimentation end-member and the solid lines show the sedimentation end-member (the shaded region denotes intermediate regimes). In Figures 5b and 5d, the dashed line depicts a segregated bed load, while the solid line depicts a well-mixed bed load condition. For all cases assuming sedimentation processes (bed load and the sedimenting suspended load condition) the volume fraction of ash approaches a steady value in the first few L' units.

4.3. Implications of End-Member Analytical Expressions for Ash Production

[29] To examine some generic features of the analytical expressions (equations (10), (13), (15), and (16)), flows were considered with heights of 100 m, pumice diameters of 1.0 cm and density of 500 kg/m^3, and ash particles produced during transport of 100 microns and density of 2000 kg/m^3. Two initial volume fractions were considered for dilute, $\alpha_2^0 = 0.025$, and denser, $\alpha_2^0 = 0.1$, conditions. Suspended load ash production and bed load ash production were considered separately using these initial conditions. We use the following dimensionless length and timescales to compare features of the flows for different flow conditions:

$$L' = \frac{L}{(HU^0/w_s)}, \tag{17}$$

And

$$t' = \frac{t}{(H/w_s)}. \tag{18}$$

The results of this analysis are shown in Figure 5, where the ratios of the volume fractions of ash to pumice particles are shown as a function of the dimensionless distance traveled. Here we use the symbol, $\bar{\alpha}_3^H$, for the volume ratio of ash produced by collisions relative to pumice, and $\bar{\alpha}_4^H$ denotes this ratio for frictionally produced ash. Figures 5a and 5b consider initially dilute conditions for the suspended load and bed load ash production, respectively, and Figures 5c and 5d consider the ash production for initially dense conditions. The dashed curves in the suspended load conditions are for the completely suspended (no settling) end-member case (equation (10)) and the solid curves account for settling via the settling velocity (equation (13)). The gray shaded region depicts the range of possibilities between these two end-member conditions. In the bed load with frictionally generated ash, the two end-members are depicted as dashed lines (for segregated bed load) and solid lines (for well-mixed bed load).

[30] As particles settle out of the suspended load the velocity decreases, reducing the rate of ash production in both the suspended load and the bed load (again assuming

that the velocity conditions of both layers are coupled). The only exception is the end-member condition for the suspended load in which no particles settle out. In all other cases the ash production asymptotes to zero as the flow velocity approaches zero.

[31] For the flow conditions examined, initially denser flows result in a greater volume fraction of ash produced relative to the initial amount of large particles present. This can be explained by the fact that the denser flows contain greater kinetic energy and lead to higher velocity. As the bed load ash production scales linearly with velocity, any increase in velocity will similarly result in greater ash production. Somewhat counterintuitively, the initially denser flows produce a smaller fraction of collisional ash than dilute conditions. However, this is because the ratio of ash to pumice is plotted; the total volume of ash is still greater in the denser flows. As more large particles are added the rate of production does not keep pace with the dilution from the added particles and the total ratio decreases. The exponential loss of particles from the suspended load due to settling removes a large fraction of the large particles before they have time for multiple collisions and ash production.

[32] The analytical model primarily addresses flows that are continually decelerating (except for the no settling case) over a level surface. The large difference in the decelerating case and the no-settling case that maintains its velocity implies that conditions that can locally accelerate the flow (e.g., going over steep slopes) may have significant effect on ash production. We examine this in detail next using numerical models.

5. Multiphase Approach to Ash Production and Transport

[33] Unsteady flows, mechanical disequilibrium, and particle clustering cannot be predicted with the analytical approach, and this motivates further numerical consideration of in situ ash production using a multiphase numerical model. We introduce a subgrid, source term based model for the production of collisional (equation (1)) and frictional ash (equation (2)) to assess the role of gas-particle decoupling, formation of large-scale structures, and varying slope conditions on the ash production budget of pyroclastic flows. The subgrid ash production model is incorporated in a continuum multiphase approach. Here, separate equations for mass, momentum, and thermal energy are solved for each mechanically distinct phase. We use the MFIX (multiphase flow with interphase exchanges) numerical approach adapted for volcanic flows [*Dufek and Bergantz*, 2007b; *Gera et al.*, 2004]. The separate phases are interpenetrating continua with volume fractions equal to unity in a control volume, similar to other continuum multiphase approaches [*Clarke et al.*, 2002; *Dartevelle et al.*, 2004; *Neri et al.*, 2002]. This code has been validated for particle-laden gravity currents through comparison to experiments and direct numerical simulations [*Dufek and Bergantz*, 2007b], and has been used to examine multiphase conduit flow [*Dufek and Bergantz*, 2005], three-dimensional column collapse and pyroclastic flow dynamics [*Dufek and Bergantz*, 2007a], and subgrid steam production when pyroclastic flows enter the sea [*Dufek et al.*, 2007].

[34] In the simulations used to examine in situ ash production, four separate phases are simulated representing the gas, pumice, collisionally produced ash, and frictionally produced ash. For each phase separate conservation equations for mass, momentum and thermal energy are solved. Although the physical properties of the collisional and friction generated ash are identical, we consider them as separate phases to identify if either phase preferentially populates different regions of the flow and to what extent the ash migrates to regions of the flow distinct from the source of the ash.

[35] The continuity equations for the gas, large particles, collisionally produced ash, and frictionally produced ash are

$$\frac{\partial}{\partial t}\left(\alpha_g \rho_g\right) + \frac{\partial}{\partial x_i}\left(\alpha_g \rho_g U_{g_i}\right) = 0, \tag{19}$$

$$\frac{\partial}{\partial t}\left(\alpha_2 \rho_2\right) + \frac{\partial}{\partial x_i}\left(\alpha_2 \rho_2 U_{2_i}\right) = \underbrace{-R_{23}}_{\substack{\text{Mass loss due to}\\ \text{collisional ash}\\ \text{prodution}}} \underbrace{-R_{24}}_{\substack{\text{Mass loss due to}\\ \text{frictional ash}\\ \text{prodution}}}, \tag{20}$$

$$\frac{\partial}{\partial t}\left(\alpha_3 \rho_3\right) + \frac{\partial}{\partial x_i}\left(\alpha_3 \rho_3 U_{3_i}\right) = \underbrace{+R_{23}}_{\substack{\text{Mass gain due to}\\ \text{collisional ash}\\ \text{prodution}}}, \tag{21}$$

and

$$\frac{\partial}{\partial t}\left(\alpha_4 \rho_4\right) + \frac{\partial}{\partial x_i}\left(\alpha_4 \rho_4 U_{4_i}\right) = \underbrace{+R_{24}}_{\substack{\text{Mass gain due to}\\ \text{frictional ash}\\ \text{prodution}}}. \tag{22}$$

The momentum equations for each phase are given as

$$\frac{\partial}{\partial t}\left(\alpha_g \rho_g U_{g_i}\right) + \frac{\partial}{\partial x_i}\left(\alpha_g \rho_g U_{g_i} U_{g_j}\right) = \frac{\partial P_g}{\partial x_i}\delta_{ij} + \frac{\partial \tau_{g_{ij}}}{\partial x_j} + I_{g_i} + \alpha_g \rho_g g_i, \tag{23}$$

$$\frac{\partial}{\partial t}\left(\alpha_2 \rho_2 U_{2_i}\right) + \frac{\partial}{\partial x_i}\left(\alpha_2 \rho_2 U_{2_i} U_{2_j}\right) = \frac{\partial P_2}{\partial x_i}\delta_{ij} + \frac{\partial \tau_{2_{ij}}}{\partial x_j} + I_{2_i} + \alpha_2 \rho_2 g_i - R_{23} U_{2_i} - R_{24} U_{2_i}, \tag{24}$$

$$\frac{\partial}{\partial t}\left(\alpha_3 \rho_3 U_{3_i}\right) + \frac{\partial}{\partial x_i}\left(\alpha_3 \rho_3 U_{3_i} U_{3_j}\right) = \frac{\partial P_3}{\partial x_i}\delta_{ij} + \frac{\partial \tau_{3_{ij}}}{\partial x_j} + I_{3_i} + \alpha_3 \rho_3 g_i + R_{23} U_{3_i}, \tag{25}$$

and

$$\frac{\partial}{\partial t}\left(\alpha_4 \rho_4 U_{4_i}\right) + \frac{\partial}{\partial x_i}\left(\alpha_4 \rho_4 U_{4_i} U_{4_j}\right) = \frac{\partial P_4}{\partial x_i}\delta_{ij} + \frac{\partial \tau_{4_{ij}}}{\partial x_j} + I_{4_i} + \alpha_4 \rho_4 g_i + R_{24} U_{4_i}. \tag{26}$$

Table 1. Symbols

Symbol	Description	Units
B	Constant in analytical model	-
$\bar{c}_p$	Heat capacity	J/kg K
d_p	Particle diameter	m
g_0	Radial distribution function	-
$\overline{H}$	Mean interphase heat transfer	J/m^3 s
H	Flow height	m
I	Interphase momentum transfer (drag)	Pa/m^3
L'	Nondimensional length	-
M	Empirical constant for frictional ash production (0.0045)	kg/m^3
m	Mass	kg
N	Empirical constant for collisional ash production (2.1×10^{-5})	s^2/m^2
P	Pressure	Pa
q	Thermal heat flux	J/m^2 s
R_{23}	Rate of collisional ash production	kg/m^3 s
R_{23}	Rate of frictional ash production	kg/m^3 s
T	Temperature	K
U_i	Velocity	m/s
Δu	Impact velocity	m/s
w_s	Settling velocity	m/s
x	Spatial position	m
Δy	Near bed region of frictional ash production	m
α	Volume fraction	-
α^{CP}	Close-packed particle volume fraction	-
ψ	Collisional ash production	kg/m^3 s
ε_c	Collisional energy dissipation	W/m^3
ξ	Rate of frictional ash production	kg/m^3 s
ϕ	Slope angle	-
μ_p	Viscosity of dilute granular material	Pa s
ρ	Density	kg/m^3
θ	Granular temperature	m^2/s^2
γ	Bed load height	m
τ_{ij}	Stress tensor	Pa

The thermal energy equations are given as

$$\alpha_g \rho_g c_p \left(\frac{\partial T_g}{\partial t} + U_{g_i} \frac{\partial T_g}{\partial x_i} \right) = \frac{\partial q_g}{\partial x_i} - \overline{H}_{g2} - \overline{H}_{g3} - \overline{H}_{g4}, \quad (27)$$

$$\alpha_2 \rho_2 c_p \left(\frac{\partial T_2}{\partial t} + U_{2_i} \frac{\partial T_2}{\partial x_i} \right) = \frac{\partial q_2}{\partial x_i} + \overline{H}_{g2}, \quad (28)$$

$$\alpha_3 \rho_3 c_p \left(\frac{\partial T_3}{\partial t} + U_{3_i} \frac{\partial T_3}{\partial x_i} \right) = \frac{\partial q_3}{\partial x_i} + \overline{H}_{g3}, \quad (29)$$

and

$$\alpha_4 \rho_4 c_p \left(\frac{\partial T_4}{\partial t} + U_{4_i} \frac{\partial T_4}{\partial x_i} \right) = \frac{\partial q_4}{\partial x_i} + \overline{H}_{g4}. \quad (30)$$

The notation is summarized in Table 1. R_{23} and R_{24} are the production rates of ash from collisional and frictional process as described in equations (7) and (3). In the continuity equation for the pumice phase (phase 2), there are two ash sink terms with negative signs to represent comminution. These sink terms are balanced by collisional ash and frictional ash source terms in equations (21) and (22). Analogous terms exist in the momentum equations because momentum is transferred from the pumice to the fine particles as the ash is being produced. In the thermal energy equation only gas-particle heat exchange is considered (i.e., heat transfer between separate particle phases is not considered).

[36] A schematic illustration of the two-dimensional model geometry is shown in Figure 6. We consider both level terrain and flow down a slope characterized by an angle (ϕ) from horizontal. The saltation boundary condition used by *Dufek and Bergantz* [2007b] is used here. The size and density of particles is identical to those adopted in the analytical models: large particles are 1.0 cm in diameter with a density of 500 kg/m^3, and ash size particles are 100 microns in diameter with a density of 2000 kg/m^3. This distribution is an obvious simplification compared to the polydisperse distribution present in pyroclastic density current deposits. The main aim of these simulations is not to emulate natural flows in detail, but rather to assess the dominant controls on ash production and resulting feedback on the dynamics of these flows. Grid resolution is refined at the base of flows and ranges from 0.1 m near the base to 10 m at the upper boundary. Horizontal resolution is 10 m. The conditions for all the simulations considered are listed in Table 2.

6. Ash Production Over Level Terrain: A Comparison With Analytical Models

[37] The conditions examined by the end-member analytical models are revisited with the multiphase numerical simulations: initially dilute conditions have a particle volume fraction of 0.025 large pumice particles, and high particle volume fraction simulations have a volume fraction of 0.10 large pumice particles. To compare directly to the analytical models, we first consider flows on level terrain and then consider flows traveling downslopes.

[38] The simulated flows over level terrain have two primary ash production zones corresponding to frictional and collisional production of ash (Figures 7, 8, and 9). In the near vent region, collisional ash produced is primarily at the top of the flow where shear is greatest. The large velocity gradients generate high granular temperatures and a concomitant increase in number of particle collisions. As the flows propagate away from the vent, the mean velocity and velocity gradients diminish as does the particle concentration in the upper region of the flow, both leading to a decrease in collisional ash production. The high velocity in the near vent region also results in the highest frictional ash production.

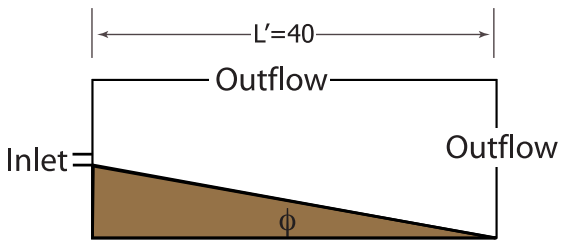

Figure 6. Schematic illustration of the model geometry. Top and right side boundaries permit outflow, and the simulations have a variable slope angle ϕ.

Table 2. Summary of Simulation Results

Initial Volume Fraction	Angle ϕ	Final Volume Fraction of Ash[a]	Collisional Ash Fraction[b]
0.025	0	.061	.56
0.025	10	.082	.69
0.025	20	.121	.80
0.025	30	.167	.82
0.10	0	.101	.10
0.10	10	.127	.47
0.10	20	.168	.69
0.10	30	.221	.77

[a]Total volume fraction of ash (including both collisional and frictional ash) relative to pumice and gas.
[b]Fraction of the ash produced by collisions relative to the total amount of ash.

[39] Wedge shaped deposits of primarily large particles form after multiple settling timescales (Figure 7) in the level terrain simulations. Although more frictional ash stays confined in the near bed region relative to collisionally produced ash, both frictional and collisional ash populate similar regions of the flow, and ash redistribution away from its source region is one of the primary differences between the analytical results and the multiphase simulation results (Figure 9). Ash generated both by collisions and friction forms a detached density gravity current that propagates to the edge of the computational domain with a runout at least four times greater than that of the pumice flow alone. In the dilute simulations, ash in the detached currents is produced in roughly equal proportions by collisions and bed friction with ~58% of the current composed of collisional ash. However, for initially dense conditions (0.1 volume fraction of particles initially) ash production is dominated by bed

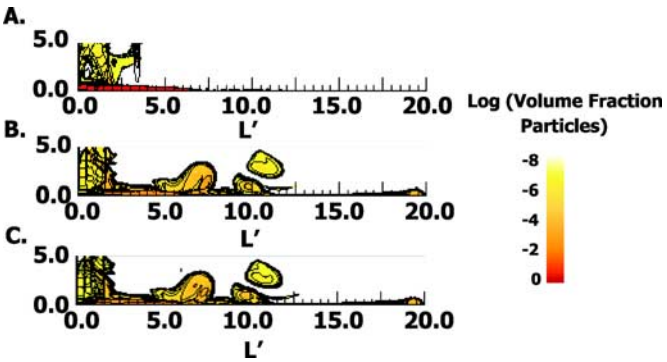

Figure 7. Simulation over level terrain. The log of the particle volume fraction is shown for the (a) 1.0 cm clasts initially introduced, (b) the collisionally produced ash, and (c) the frictionally produced ash at time $t' = 70$. At this time snapshot the 1.0 cm particles have formed a wedge-shaped deposit, and the produced fines have formed a detached gravity current that is continuing to propagate. Although the ash from the collisional and frictional processes is generated in different regions of the flow, significant fractions of both populations form the outgoing density current. The head of the outgoing current is composed of ~58% collisionally produced ash and ~42 % frictionally produced ash.

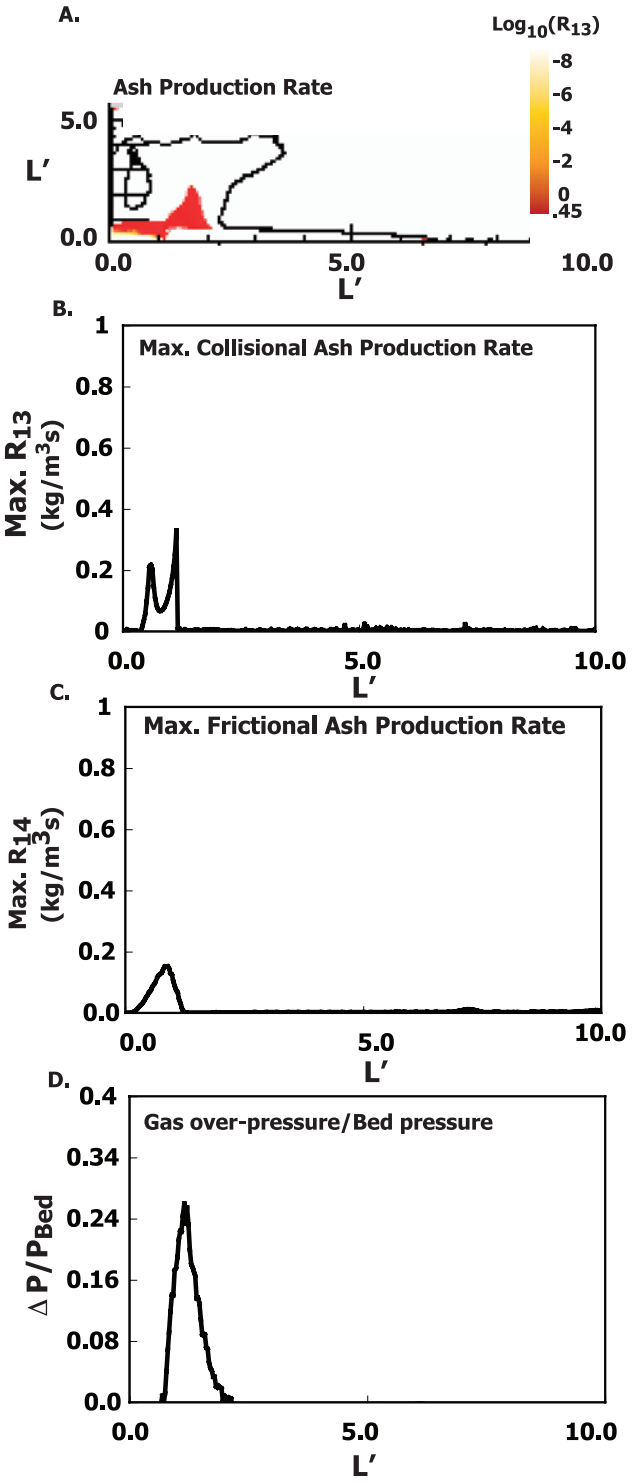

Figure 8. Rate of production of ash in flow over level terrain (initial volume fraction of 0.025). (a) Log of the collisional ash production rate. (b) Maximum rate of ash production at different distances from flow inlet. Collisionally produced ash is primarily produced in the high shear zones near the top of the current, near the flow inlet. (c) Maximum rate of frictionally produced ash. (d) Gas overpressure relative to atmospheric pressure, normalized by the weight of the bed particles.

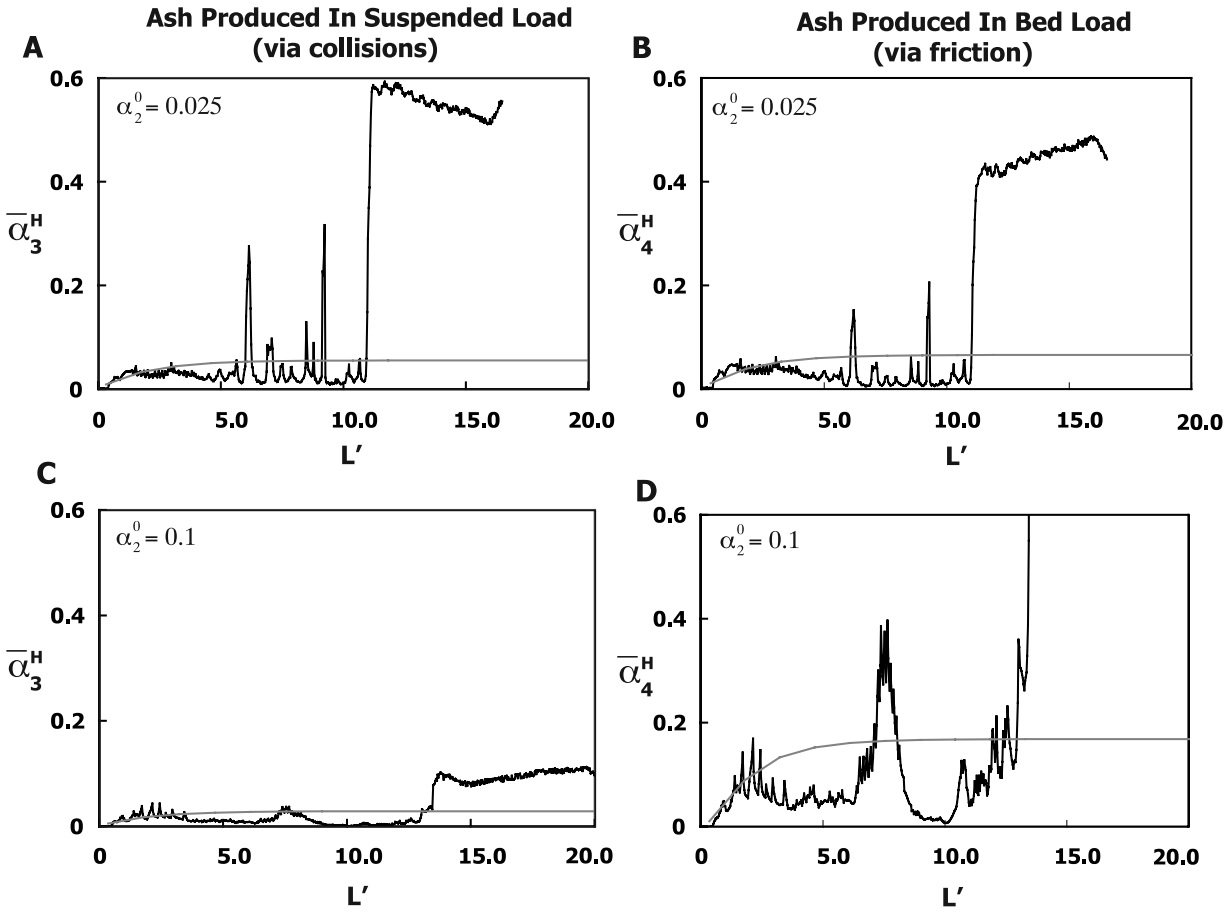

Figure 9. Comparison of the numerical simulations (dark solid lines) and analytical models (light gray lines) for initially dilute and dense conditions. In the diagram, $\overline{\alpha}_3{}^H$ indicates the volume ratio of ash produced by collisions relative to pumice (vertically averaged), and $\overline{\alpha}_4{}^H$ denotes this ratio for frictionally produced ash. (a and b) The suspended load and bed load calculations for the dilute ($\alpha_2{}^0 = 0.025$) case, respectively. (c and d) The suspended load and bed load calculations for the denser ($\alpha_2{}^0 = 0.1$) case, respectively. These simulations and calculations are for level terrain ($\phi = 0°$). Although the analytical and multiphase simulations show similar trends, the advection and segregation of ash into large-scale structures in the simulations produces notable differences. In all four cases a detached current composed of ash from friction and collisions continues to propagate further than the mostly sedimented 1.0 cm clasts. Also, entrainment and Kelvin-Helmholtz billows produce most of the fluctuations relative to the analytical solution.

friction, and frictional ash results in the majority, ~74%, of the ash in the detached currents.

7. Ash Production Within Flows Traveling Downslopes

[40] The conversion of potential energy to kinetic energy for flows descending slopes drives the enhanced production of ash by both frictional and collisional processes. Figures 10 and 11 illustrate ash dispersion and production rates for flows descending 30 degree slopes. In the 30 degree slope case the flows are nondepositional, and all the large particles initially present at the flow inlet are continually subjected to collisions or frictional abrasion. The ash produced does not form an independent, detached current, but moves with the bulk of the flow because even the pumice remains mobile for these steep slopes.

[41] Collisional ash production is concentrated in the head of the gravity current. The high particle concentrations and strong coherent vortical motion in the head of the current enhances ash production by increasing the number and energy of the collisions. Collisional ash production rates of over 0.8 kg/m^3 s are reached in the head of the current but quickly decay in the tail of the current (Figure 11). This should lead to greater rounding of pumice in the snout of flows descending steep slopes. The nearly constant basal velocity of the current results in nearly uniform rates of ash production from frictional sources, with production rates of ~0.15 ± 0.05 kg/m^3 s along the entire length of the flow. Again, although collision and friction-generated ash are produced in spatially and temporally distinct regions of the flow, the distribution of the ash is typically not confined to the source region.

8. Implications of In Situ Ash Production

[42] In situ ash production increases the effective runout distance on low angle slopes by producing detached cur-

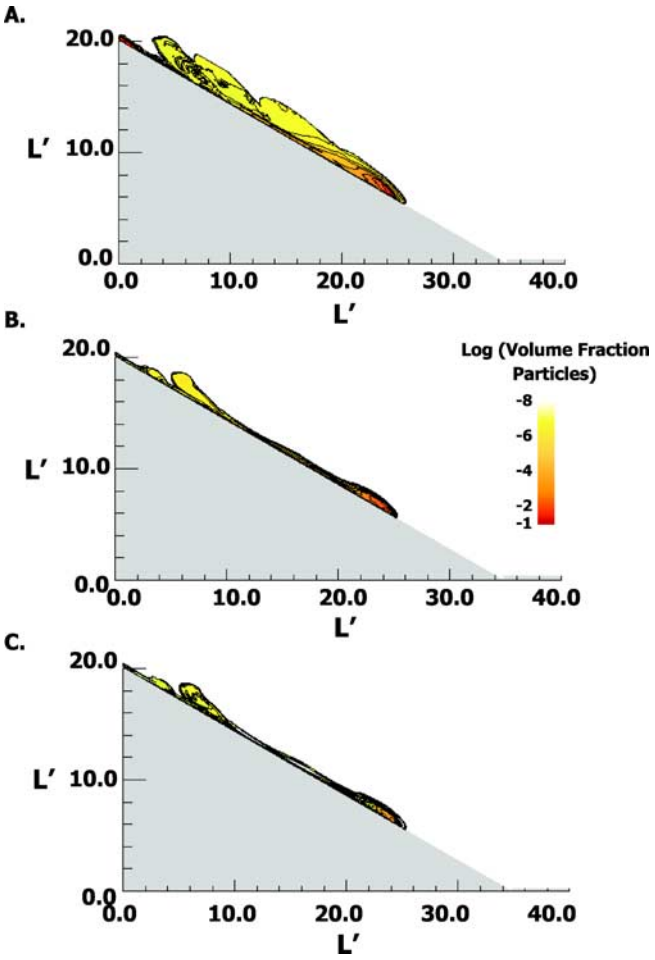

Figure 10. Volume fraction of particles in a flow descending a 30° slope at $t' = 8$. This flow initially had a volume fraction of 0.025. (a) The volume fraction of 1.0 cm particles. (b) The volume fraction of collisionally produced ash and (c) the volume fraction of frictionally produced ash.

rents that are entirely composed of segregated ash. Flows that have ash-sized particles from the initial fragmentation may also produce similar features independent of in situ ash. However, the volume of ash and velocity of these detached currents will increase if in situ ash production occurs in a flow. Using a specified Froude number head condition, equation (9) shows that doubling the volume fraction of ash results in a ~41% increase in the detached current front velocity. In the simulations, flows that descended steep slopes (~30 degrees) did not produce detached currents of ash because the constant slope allowed the pumice to continue to travel across the entire simulation domain. Under natural conditions a break in slope would also likely result in detached currents, and steeper initial conditions that enhance ash production would produce more voluminous detached currents [*Bourdier and Abdurachman*, 2001; *Calder et al.*, 1999; *Fujii and Nakada*, 1999].

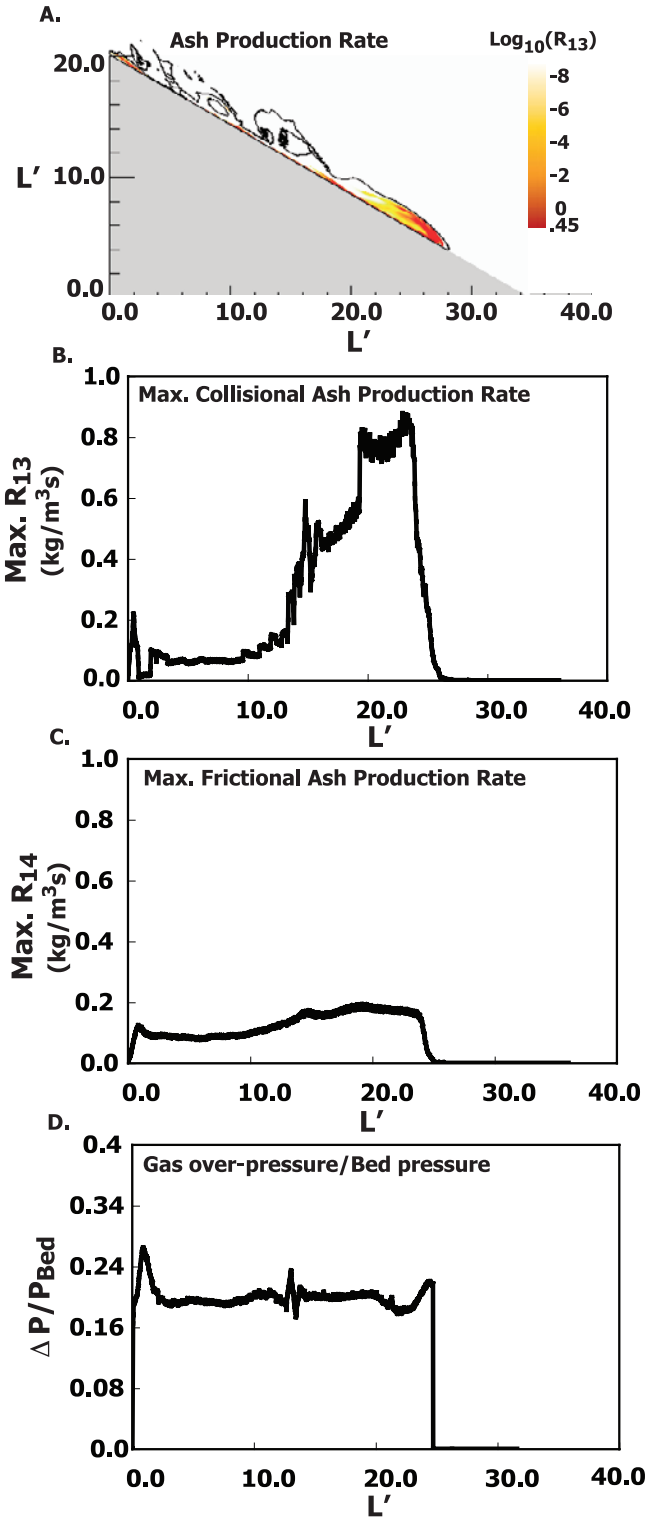

Figure 11. Rate of production of ash for a flow descending a 30° slope. The flow initially has a particle volume fraction of 0.025. (a) The production rate of collisionally produced ash. The majority of the collisionally produced ash is produced in the head of the gravity current. (b) The maximum ash production rate at different distances from the flow source. (c) The rate of production of frictionally produced ash. The nearly constant rate of production of frictionally generated ash is consistent with near-uniform bed load velocities in this flow. (d) The pressure above atmospheric pressure normalized by the bed pressure.

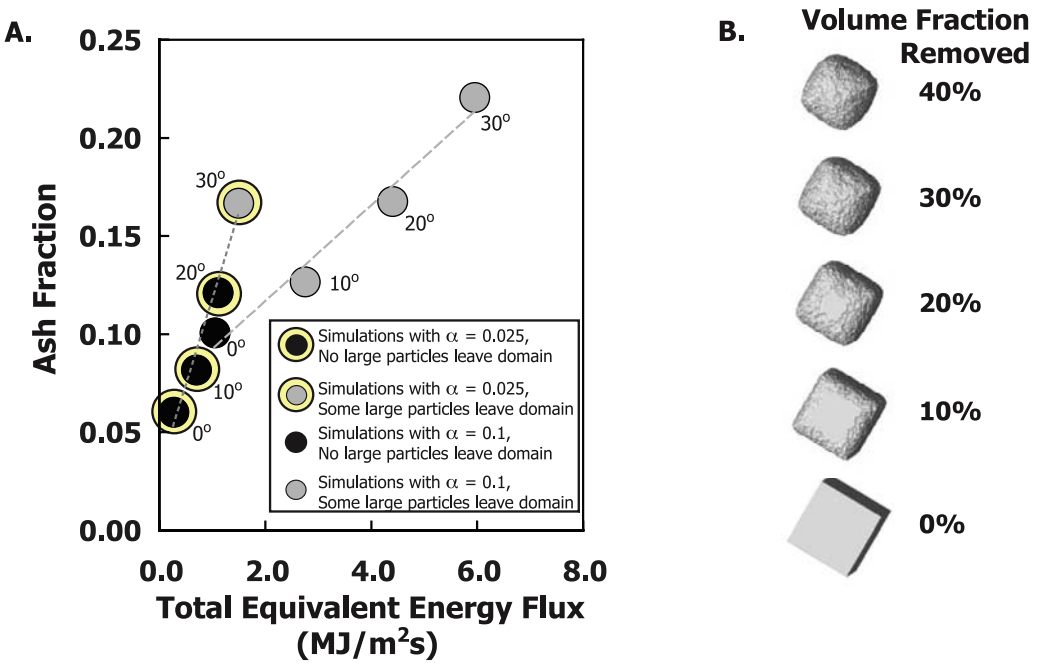

Figure 12. (a) Total fraction of the flow that is ash after either deposition or flow has transited $L' = 40$ versus the energy flux in the system. The energy flux includes both the kinetic and potential energy contributions. All flows initially had no ash and were composed of 1.0 cm pumice particles. Black circles denote conditions that produced deposits, and gray circles depict flows that had some centimeter particles transit the computational domain (nondepositional) owing to steep slopes. Yellow haloes around the symbols indicate dilute initial conditions ($\alpha = 0.025$ volume fraction). The angle of the slope is noted next to the symbol. The two different volume fraction initial conditions form separate trends, each with ash production increasing roughly linearly with increasing energy flux. (b) Illustration of particle roundness as a function of volume percent removed by comminution. These plots were generated assuming the probability for removing an increment of volume scales linearly with the exposed surface area. Volume increments considered were 0.0001% of the total volume.

[43] In the numerical simulations, pore pressure at the base of the flow never reached the total bed weight. However, in flows with complex particle size distributions we would anticipate that the initial permeability would be lower. Under those conditions higher pore pressures would be expected compared to the initially coarse distribution considered here. Nevertheless, flows descending slopes did produce pore pressures that could accommodate about 20% of the weight for most of the flow length. Under decelerating flow conditions, such as a break in slope, the pore pressure conditions would begin to dissipate leading to late sorting and elutriation of fine particles.

[44] The ash production simulation results are summarized in Figure 12. The total fraction of ash relative to pumice is shown at the moment any material leaves the simulation domain. We note that for the low angle case, the large, pumice particles in the flow have reached their final runout, and ash production ceases at this point. However, for the high-angle simulations where pumice particles exit the domain, even greater ash production may be expected if the simulation domain were larger. For the type of particles considered in the simulations, $L' = 40$ corresponds to length scales of approximately 10 km. The volume fraction of ash produced is plotted as a function of the total equivalent energy flux (which includes contributions from the mean and fluctuating kinetic energy and the gravitational potential energy). As the initial velocity of these currents was held fixed in these simulations, higher energy flows either correspond to higher volume fraction of particles or greater potential energy from steep slopes. Larger energy flux results in greater volume fractions of ash in general, although the two different initial volume fractions of pumice produced separate trends with the more voluminous and higher energy flows producing greater fractions of ash.

[45] Near vent and steady to accelerating flow conditions are responsible for the majority of the ash produced in the simulations. For small volume flows, the rapid descent down volcanic edifices promotes in situ ash production. The Mount St. Helens flow shown in Figure 1 is an example of such a flow. The ash produced during these downhill flows can feed secondary columns and are likely components of dilute currents that detach from these flows at topographic barriers or changes in slope. Although we do not specifically address very large volume flows, we infer that the near vent, column collapse region of the flow would produce the greatest ash in caldera forming eruptions.

[46] The flow configurations examined here are simplified compared to natural flows, but the general features of the results explain many qualitative and quantitative field observations. Glass rim and crystal abrasion observations [e.g., *Freundt and Schmincke*, 1992; *Taddeucci and Palladino*, 2002] indicate that pyroclastic flow transport can lead to abrasion of particles, most likely in near vent regions.

[47] Unfortunately, detailed, quantitative studies of the roundness of pumice in deposits are limited. We note that extensive comminution is required to produce particles typically described as well rounded, with most deposits in this category associated with >30% volume reduction (Figure 12). The deposits from most of the flows examined in this study would be described as subangular to rounded in most sedimentological classification schemes [*Compton*, 1985; *Powers*, 1953; *Tucker*, 1982].

9. Summary

[48] The in situ production of fine particles by comminution and abrasion in propagating pyroclastic density currents contributes to the ash component and rounding of particles preserved in deposits. Ash production is most likely to occur in high-energy, near-vent regions of the flow as well as where flows descend steep slopes. In both instances, ash production is maximized in nondepositional settings. The produced ash can decouple from the flow during a decelerating phase of transport such as after a break in slope. For most flow conditions the fraction of pumice comminuted to ash is in the range of 10–20% of the volume of pumice. The produced ash increases the effective runout and mobility of the current and also leads to higher pore pressures in the body of the flow. Ash from both frictional and collisional sources is likely well mixed with ash from conduit sources. Hence understanding the contribution from in situ ash on the grain size distribution will help us better constrain conduit processes. Our coupled experiment and modeling approach suggests that the degree of rounding and abrasion is linked to the dynamics of transport and may be a useful tool for estimating total ash production. Further work on integrating crystal-scale abrasion measurements and quantitative measurements of the roundness of particles (in experiments and in deposits) are needed to integrate measurements made on deposits with our numerical and experimental results.

Appendix A: Subgrid Model for Collisional Ash Production

[49] The production of ash by collisions is given by the product of the collision frequency, mass fraction of ash produced per collision, and the mass of each particle

$$R_{23} = \underbrace{\frac{144(\alpha_2)^2\sqrt{\theta}g_0}{\pi^{3/2}(d_2)^4}}_{\text{Collision Frequency}} \times \underbrace{\psi(\Delta\bar{u})}_{\substack{\text{Mass Fraction}\\ \text{of ash per}\\ \text{collision}}} \times \underbrace{\frac{\rho_2\pi(d_2)^3}{6}}_{\text{Mass per particle}}, \tag{A1}$$

where α_2 is the particle volume fraction, θ is the granular temperature, d_2 is the particle diameter, and $\Delta\bar{u}$ is the average impact velocity. Again, the subscripts designate the phase, where phase 2 refers to pumice particles, 3 refers to collisionally produced ash and 4 refers to frictionally produced ash. The radial distribution function, g_0, is given by [*Gidaspow*, 1994]

$$g_0 = \left[1 - \left(\frac{\alpha_2}{\alpha_2^0}\right)^{1/3}\right]^{-1}. \tag{A2}$$

To determine the average impact velocity ($\Delta\bar{u}$), we first need to determine the probability distribution for impact velocities, and then integrate over all possibilities to determine the average impact velocity.

[50] The joint probability distribution for impact velocity is given as

$$f_{\Delta u} = \int_{-\infty}^{\infty} \left[\frac{1}{\sqrt{2\pi\theta}}\exp\left[\frac{-c^2}{2\theta}\right]\right]\left[\frac{1}{\sqrt{2\pi\theta}}\exp\left[\frac{-(c+\Delta u)^2}{2\theta}\right]\right] dc = \frac{1}{2\sqrt{\pi\theta}}\exp\left[\frac{-\Delta u^2}{4\theta}\right]. \tag{A3}$$

Using the joint probability distribution we determine the average velocity at impact

$$\Delta\bar{u} = \int_0^{\infty} \Delta u \frac{1}{2\sqrt{\pi\theta}}\exp\left[\frac{-\Delta u^2}{4\theta}\right] d\Delta u = \sqrt{\theta/\pi}. \tag{A4}$$

Using

$$\psi(\Delta u) = N\Delta u^2, \tag{A5}$$

where $N = 2.1 \times 10^{-5}$ s^2/m^2 from the experiments, we obtain

$$R_{23} = \frac{24(^2\alpha)^2\theta^{3/2}N(^2\rho)g_0}{\pi^{3/2}(^2d)}. \tag{A6}$$

Appendix B: Frictional Production of Ash

[51] The rate of frictional ash production is

$$R_{24} = \frac{1}{\Delta y}\xi(u), \tag{B1}$$

Where

$$\xi(u) = Mu, \tag{B2}$$

and $M = 0.0045$ kg/m^3 is determined from the experiments of *Cagnoli and Manga* [2004]. The experimentally derived relationship for the frictional production of ash gives the mass of ash produced per unit area per second. In practice, we will introduce the ash in the basal control volumes, which have a resolution of Δy. As the grid will be refined at the base, this should only introduce small errors.

Appendix C: Analytical Model of Collisional Ash Production

[52] An analytical model was constructed to predict the ash production in a suspended load layer (by particle collisions) and in a bed load region (particle abrasion). Here, phase 1 refers to the gas phase, phase 2 refers to large particles, phase 3 refers to ash generated by collisions, phase 4 refers to ash generated by frictional interactions.

[53] We assume the particle loss in suspended load is due to settling (w_s) from suspended load region to bed load region. The incremental loss is given by

$$\alpha_2^s = \frac{\alpha_2^0 w_s dt}{H}, \tag{C1}$$

so that

$$\alpha_2^S = \alpha_2^0 \exp\left[\frac{-w_s t}{H}\right]. \tag{C2}$$

[54] The thickness of the bed load region (where the volume fraction is close packed, α^{CP}) can be found by rearranging the relation

$$\alpha_2^0 H = \alpha_2^0 \exp\left[\frac{-w_s t}{H}\right][H-\gamma] + \alpha^{CP}\gamma \tag{C3}$$

to give

$$\gamma = \frac{\alpha_2^0 H\left(1-\exp\left[\frac{-w_s t}{H}\right]\right)}{\alpha^{CP} - \alpha_2^0 \exp\left[\frac{-w_s t}{H}\right]}. \tag{C4}$$

To determine collisional ash production, we need an estimate for granular temperature (to determine the probability of collisions and the average impact velocity). Here we assume that the rate of production of granular temperature by shear is balanced by dissipation by inelastic collisions (this neglects wall-particle dissipation because this is suspended load, and neglects dissipation by the fluid), that is

$$\mu_p\left(\frac{\partial U}{\partial y}\right)^2 = \varepsilon_c. \tag{C5}$$

The energy dissipation, ε_c, is equal to the product of the number of collisions and energy lost per collision. The energy dissipation is

$$\varepsilon_c = \frac{144\left(\alpha_2^s\right)\sqrt{\theta g_0}}{\pi^{3/2} d_2^4}\left(\left[\frac{1}{2}m_2[\Delta u]^2\right] - \left[\frac{1}{2}m_2[\Delta u e]^2\right]\right), \tag{C6}$$

because

$$m_2 = \frac{\pi}{6} d_2^3\ \rho_2. \tag{C7}$$

Equation (C6) can be expressed as

$$\varepsilon_c = \frac{12\left(\alpha_2^s\right)\sqrt{\theta g_0}\Delta u^2(1-e^2)\rho_2}{\pi^{1/2} d_2}. \tag{C8}$$

From Appendix A,

$$\Delta u = \sqrt{\theta/\pi}. \tag{C9}$$

Using equation (C9) and the expression for dilute granular flow viscosity from Chapman and Cowling in equation (C5), and solving for the granular temperature gives

$$\theta = \frac{5\pi^2 d_2^2}{1152\left(\alpha_2^s\right)^2(1-e^2)}\left(\frac{\partial U}{\partial y}\right)^2. \tag{C10}$$

We can estimate the mean velocity derivative by assuming

$$\frac{\partial U}{\partial y} \approx \frac{2U}{H}. \tag{C11}$$

Assuming the densimetric Froude number of the front of the current is approximately $\sqrt{2}$, the front velocity is

$$U = \sqrt{\frac{2\alpha_p\left(\rho_p - \rho_1\right)gH}{\rho_1}}. \tag{C12}$$

Here α_p denotes the volume fraction of all particles in the flow. Using equations (C9) and (C11) in equation (C10) provides an approximation for the granular temperature of the suspended load portion of the flow

$$\theta = \frac{5\pi^2 d_2^2 \alpha_p(\rho_2 - \rho_1)g}{144\alpha_2^2(1-e^2)H\rho_1}. \tag{C13}$$

If sedimentation occurs, α_p is a function of time. We consider two cases for the suspended load: (1) no sedimentation out of the layer (α_p is constant) or (2) sedimentation of big particles out of suspended load given by the settling velocity (Assume on these timescales produced ash always stays in the suspended load).

[55] In the first case,

$$d\alpha_3^S = \frac{R_{23}}{\rho_3} dt. \tag{C14}$$

Using the expression for R_{23}, including the approximation of granular temperature and integrating gives

$$\alpha_3^s = \alpha_p - \sqrt{\alpha_p^2 - 2\left[\frac{24N}{\pi^{3/2}d^2}\right]\left[\frac{5\pi^2 d_2^2 \alpha_p(\rho_2-\rho_1)g}{144(1-e^2)H\rho_1}\right]^{3/2} t}. \tag{C15}$$

Here we will group the following constants into a single constant B

$$B = \left[\frac{24N}{\pi^{3/2}d^2}\right]\left[\frac{5\pi^2 d_2^2 \alpha_p(\rho_2-\rho_1)g}{144(1-e^2)H\rho_1}\right]^{3/2}, \tag{C16}$$

so that

$$\alpha_3^s = \alpha_p - \sqrt{\alpha_p^2 - 2Bt}. \tag{C17}$$

This is only appropriate for

$$t < \frac{\alpha_p}{2B}. \tag{C18}$$

For the second case where we assume pumice can sediment out of suspended load,

$$U = \sqrt{\frac{2(\rho_2 - \rho_1)gH\alpha_2^0}{\rho_1}} \exp\left[\frac{-w_s t}{2H}\right]. \quad \text{(C19)}$$

This yields an expression for the granular temperature

$$\theta = \frac{20\pi^2 d_2^2 \left[\frac{2(\rho_2 - \rho_1)gH\alpha_2^o}{\rho_1}\right]}{1152(1-e^2)H^2} \left[\frac{\exp\left[\frac{-w_s t}{H}\right]}{\left(\alpha_2^0 \exp\left[\frac{-w_s t}{H}\right] - \alpha_3\right)^2}\right]. \quad \text{(C20)}$$

The concentration of particles is thus

$$\alpha_3 = \frac{2H}{w_s \alpha_s^0}\left[\frac{24N}{\pi^{3/2} d_2}\right]\left(\frac{5\pi^2 d_2^2(\rho_2 - \rho_1)g\alpha_2^0}{144(1-e^2)\rho_1 H}\right)^{3/2}\left(1 - \exp\left[\frac{-w_s t}{2H}\right]\right) \quad \text{(C21)}$$

or

$$\alpha_3 = \frac{2H}{w_s \alpha_2} B\left(1 - \exp\left[\frac{-w_s t}{2H}\right]\right). \quad \text{(C22)}$$

Appendix D: Analytical Model of Bed Load Ash Production

[56] For bed load ash production two end-members are also evaluated assuming: (1) all big particles make it to the very bottom of flow where they can produce ash efficiently and (2) all particles in the bed load are well mixed (this reduces the concentration of large particle n the bed load and results in less efficient ash production).

[57] In the first case,

$$d\alpha_4 = \frac{R_{24}}{\rho_2} dt. \quad \text{(D1)}$$

When phase 2 is exhausted it can no longer produce ash.

[58] For the second assumption,

$$d\alpha_4 = \frac{R_{24}}{\rho_2}\left(\frac{\alpha_2}{\alpha_{CP}}\right) dt. \quad \text{(D2)}$$

Also note that, by definition, in the bed load $\alpha_{CP} = \alpha_2 + \alpha_4$. From the experiments,

$$R_{24} = \frac{MU}{l}, \quad \text{(D3)}$$

where l is a small length scale above the bed where ash is produced. On the basis of the experiments we assume that $l \approx 5d_2$.

[59] Similar to the suspended load scaling we will use the velocity scaling

$$U = \sqrt{\frac{2(\rho_2 - \rho_1)gH\alpha_2^0}{\rho_1}} \exp\left[\frac{-w_s t}{2H}\right]. \quad \text{(D4)}$$

This assumes that bed load is traveling at the same speed as the suspended load. This bounds the solutions because in most situations the velocity will be smaller.

[60] Combining equations (D4) and (D1) gives the ash produced when all the pumice segregates to the base of the bed load

$$\alpha_4 = \left(1 - \exp\left[\frac{-w_s t}{2H}\right]\right)\frac{2HM}{w_s \rho_2 l}\sqrt{\frac{2(\rho_2 - \rho_1)gH\alpha_2^0}{\rho_1}} \approx \left(1 - \exp\left[\frac{-w_s t}{2H}\right]\right)\frac{2HM}{w_s \rho_2 5d_2}\sqrt{\frac{2(\rho_2 - \rho_1)gH\alpha_2^0}{\rho_1}}. \quad \text{(D5)}$$

Integrating the second case, equation (D2), yields the relation for a well mixed, bed load

$$\alpha_4 = \alpha^{CP}\left[1 - \exp\left(\frac{-2HM}{\alpha^{CP} w_s \rho_2 l}\sqrt{\frac{2(\rho_2 - \rho_1)gH\alpha_2^0}{\rho_1}}\right) \cdot \left(1 - \exp\left[\frac{-w_s t}{2H}\right]\right)\right] \approx \alpha^{CP}\left[1 - \exp\left(\frac{-2HM}{\alpha^{CP} w_s \rho_2 5d_2}\sqrt{\frac{2(\rho_2 - \rho_1)gH\alpha_2^0}{\rho_1}}\right) \cdot \left(1 - \exp\left[\frac{-w_s t}{2H}\right]\right)\right]. \quad \text{(D6)}$$

[61] **Acknowledgments.** We thank Daniel Standish and Bruno Cagnoli for performing many of the experiments reported here and Tim Teague for SEM assistance. We thank Sarah Fagents and two anonymous reviewers for their constructive suggestions. This work was supported by NSF Grants 0809321 (J.D.) and 0809564 (M.M.) and the Miller Institute for Basic Research in Science.

References

Allen, S. R. (2001), Reconstruction of a major caldera-forming eruption from pyroclastic deposit characteristics: Kos Plateau Tuff, eastern Aegean Sea, *J. Volcanol. Geotherm. Res.*, *105*, 141–162, doi:10.1016/S0377-0273(00)00222-5.

Bourdier, J. L., and E. K. Abdurachman (2001), Decoupling of small-volume pyroclastic flows and related hazards at Merapi volcano, Indonesia, *Bull. Volcanol.*, *63*, 309–325, doi:10.1007/s004450100133.

Britter, R. E., and J. E. Simpson (1978), Experiments on the dynamics of gravity current head, *J. Fluid Mech.*, *88*, 223–240, doi:10.1017/S0022112078002074.

Bursik, M., and A. Woods (1996), The dynamics and thermodynamics of large ash flows, *Bull. Volcanol.*, *58*, 175–193, doi:10.1007/s004450050134.

Cagnoli, B., and M. Manga (2003), Pumice-pumice collisions and the effect of the impact angle, *Geophys. Res. Lett.*, *30*(12), 1636, doi:10.1029/2003GL017421.

Cagnoli, B., and M. Manga (2004), Granular mass flows and Coulomb's friction in shear cell experiments; Implications for geophysical flows, *J. Geophys. Res.*, *109*, F04005, doi:10.1029/2004JF000177.

Calder, E. S., P. D. Cole, W. B. Dade, T. H. Druitt, R. P. Hoblitt, H. E. Huppert, L. Ritchie, R. S. J. Sparks, and S. R. Young (1999), Mobility of pyroclastic flows and surges at the Soufriere Hills Volcano, Montserrat, *Geophys. Res. Lett.*, *26*, 537–540, doi:10.1029/1999GL900051.

Calder, E. S., R. S. J. Sparks, and M. C. Gardeweg (2000), Erosion, transport and segregation of pumice and lithic clasts in pyroclastic flows inferred from ignimbrite at Lascar Volcano, Chile, *J. Volcanol. Geotherm. Res.*, *104*, 201–235, doi:10.1016/S0377-0273(00)00207-9.

Chapman, S., and T. G. Cowling (1952), *The Mathematical Theory of Non-Uniform Gases: An Account of the Kinetic Theory of Viscosity, Thermal Conduction, and Diffusion in Gases*, Cambridge Univ. Press, New York.

Clarke, A. B., B. Voight, A. Neri, and G. Macedonio (2002), Transient dynamics of vulcanian explosions and column collapse, *Nature*, *415*, 897–901, doi:10.1038/415897a.

Cole, P. D., E. S. Calder, R. S. J. Sparks, A. B. Clarke, T. H. Druitt, S. R. Young, R. A. Herd, C. L. Harford, and G. E. Norton (2002), Deposits from the dome-collapse and fountain-collapse pyroclastic flows at Soufrière Hills Volcano, Montserrat, *Geol. Soc. London Mem.*, *21*, 231–262.

Compton, R. R. (1985), *Geology in the Field*, 398 pp. John Wiley, New York.

Dade, W. B., and H. E. Huppert (1995), Runout and fine-sediment deposits of axisymmetric turbidity currents, *J. Geophys. Res.*, *100*, 18,597–18,609, doi:10.1029/95JC01917.

Dartevelle, S., W. I. Rose, J. Stix, K. Kelfoun, and J. W. Vallance (2004), Numerical modeling of geophysical granular flows: 2. Computer simulations of plinian clouds and pyroclastic flows and surges, *Geochem. Geophys. Geosyst.*, *5*, Q08004, doi:10.1029/2003GC000637.

Dingwell, D. B. (1996), Volcanic dilemma: Flow or blow?, *Science*, *273*, 1054–1055, doi:10.1126/science.273.5278.1054.

Dufek, J. D., and G. W. Bergantz (2005), Transient two-dimensional dynamics in the upper conduit of a rhyolitic eruption: A comparison of the closure models for the granular stress, *J. Volcanol. Geotherm. Res.*, *143*, 113–132, doi:10.1016/j.jvolgeores.2004.09.013.

Dufek, J., and G. W. Bergantz (2007a), Dynamics and deposits generated by the Kos Plateau Tuff eruption: Controls on basal particle loss on pyroclastic flow transport, *Geochem. Geophys. Geosyst.*, *8*, Q12007, doi:10.1029/2007GC001741.

Dufek, J., and G. W. Bergantz (2007b), Suspended load and bed-load transport of particle-laden gravity currents: The role of particle-bed interaction, *Theor. Comput. Fluid Dyn.*, *21*, 119–145, doi:10.1007/s00162-007-0041-6.

Dufek, J., M. Manga, and M. Staedter (2007), Littoral blasts: Pumice-water heat transfer and the conditions for steam explosions when pyroclastic flows enter the ocean, *J. Geophys. Res.*, *112*, B11201, doi:10.1029/2006JB004910.

Edmonds, M., R. A. Herd, and M. H. Strutt (2006), Tephra deposits associated with a large lava dome collapse, Soufriere Hills Volcano, Montserrat, 12–15 July 2003, *J. Volcanol. Geotherm. Res.*, *153*, 313–330, doi:10.1016/j.jvolgeores.2005.12.008.

Fisher, R. V. (1963), Bubble-wall texture and its significance, *J. Sediment. Res.*, *33*, 224–227.

Fisher, R. V., H. X. Glicken, and R. P. Hoblitt (1987), May 18, 1980, Mount St. Helens deposits in south Coldwater Creek, Washington, *J. Geophys. Res.*, *92*, 10,267–10,283, doi:10.1029/JB092iB10p10267.

Freundt, A., and H. U. Schmincke (1992), Abrasion in pryoclastic flows, *Geol. Rundsch.*, *81*, 383–389.

Fujii, T., and S. Nakada (1999), The 15 September 1991 pyroclastic flows at Unzen Volcano (Japan), a flow model for associated ash-cloud surges, *J. Volcanol. Geotherm. Res.*, *89*, 159–172, doi:10.1016/S0377-0273(98)00130-9.

Gardner, J. E., R. M. E. Thomas, C. Jaupart, and S. Tait (1996), Fragmentation of magma during Plinian volcanic eruptions, *Bull. Volcanol.*, *58*, 144–162, doi:10.1007/s004450050132.

Gera, D., M. Syamlal, and T. J. O'Brien (2004), Hydrodynamics of particle segregation in fluidized beds, *Int. J. Multiphase Flow*, *30*, 419–428, doi:10.1016/j.ijmultiphaseflow.2004.01.003.

Gidaspow, D. (1994), *Multiphase Flow and Fluidization: Continuum and Kinetic Theory Descriptions*, Academic, Boston, Mass.

Gonnermann, H. M., and M. Manga (2003), Explosive volcanism may not be an inevitable consequence of magma fragmentation, *Nature*, *426*, 432–435, doi:10.1038/nature02138.

Heiken, G., and K. Wohletz (1985), *Volcanic Ash*, Univ. of Calif Press, Berkeley.

Horwell, C. J., and P. J. Baxter (2006), The respiratory health hazards of volcanic ash: A review for volcanic risk mitigation, *Bull. Volcanol.*, *69*, 1–24, doi:10.1007/s00445-006-0052-y.

Inaoka, H., and M. Ohno (2003), New universality class of impact fragmentation, *Fractals*, *11*, 369–376, doi:10.1142/S0218348X0300221X.

Kaminski, E., and C. Jaupart (1998), The size distribution of pyroclasts and the fragmentation sequence in explosive volcanic eruptions, *J. Geophys. Res.*, *103*, 29,759–29,779, doi:10.1029/98JB02795.

Miller, T. P., and R. L. Smith (1977), Spectacular mobility of ash flows around Aniakchak and Fisher calderas, Alaska, *Geology*, *5*, 173–176, doi:10.1130/0091-7613(1977)5<173:SMOAFA>2.0.CO;2.

Neri, A., A. Di Muro, and M. Rosi (2002), Mass partition during collapsing and transitional columns by using numerical simulations, *J. Volcanol. Geotherm. Res.*, *115*, 1–18, doi:10.1016/S0377-0273(01)00304-3.

Papale, P. (1999), Strain-induced magma fragmentation in explosive eruptions, *Nature*, *397*, 425–428, doi:10.1038/17109.

Perkins, M. E., and B. P. Nash (2002), Explosive silicic volcanism of the Yellowstone hotspot: The ash fall tuff record, *Geol. Soc. Am. Bull.*, *114*, 367–381, doi:10.1130/0016-7606(2002)114<0367:ESVOTY>2.0.CO;2.

Powers, M. C. (1953), A new roundness scale for sedimentary particles, *J. Sediment. Res.*, *23*, 117–119.

Schwarzkopf, L. M., O. Spieler, B. Scheu, and D. B. Dingwell (2007), Fall-experiments on Merapi basaltic andesite and constraints on the generation of pyroclastic surges, *eEarth*, *2*, 1–5.

Self, S. (2006), The effects and consequences of very large explosive volcanic eruptions, *Philos. Trans. R. Soc. Ser. A*, *364*, 2073–2097.

Simpson, J. E. (1997), *Gravity Currents in the Environment and the Laboratory*, 2nd ed., 244 pp., Cambridge Univ. Press, Cambridge, U. K.

Sparks, R. S. J., and L. Wilson (1976), A model for the formation of ignimbrite by gravitational column collapse, *J. Geol. Soc.*, *132*, 441–452, doi:10.1144/gsjgs.132.4.0441.

Spieler, O., M. Alidibirov, and D. B. Dingwell (2003), Grain-size characteristics of experimental pyroclasts of 1980 Mount St. Helens cryptodome dacite: Effects of pressure drop and temperature, *Bull. Volcanol.*, *65*, 90–104.

Taddeucci, J., and D. M. Palladino (2002), Particle size-density relationships in pyroclastic deposits: Inferences for emplacement processes, *Bull. Volcanol.*, *64*, 273–284, doi:10.1007/s00445-002-0205-6.

Tucker, M. E. (1982), *Sedimentary Rocks in the Field*, 2nd ed., 153 pp., John Wiley, New York.

Valentine, G. A., and K. H. Wohletz (1989), Numerical models of Plinian eruption columns and pyroclastic flows, *J. Geophys. Res.*, *94*, 1867–1887, doi:10.1029/JB094iB02p01867.

Walker, G. P. L. (1981), Generation and dispersal of fine ash and dust by volcanic eruptions, *J. Volcanol. Geotherm. Res.*, *11*, 81–92, doi:10.1016/0377-0273(81)90077-9.

Wilson, C. J. N., and W. Hildreth (1997), The Bishop Tuff: New insights from eruptive stratigraphy, *J. Geol.*, *105*, 407–439.

Wohletz, K., M. F. Sheridan, and W. K. Brown (1989), Particle-size distributions and the sequential fragmentation tranport-theory applied to volcanic ash, *J. Geophys. Res.*, *94*, 15,703–15,721, doi:10.1029/JB094iB11p15703.

Zhang, Y. X. (1999), A criteria for the fragmentation of bubbly magma based on brittle failure theory, *Nature*, *402*, 648–650, doi:10.1038/45210.

Zimanowski, B., K. Wohletz, P. Dellino, and R. Buttner (2003), The volcanic ash problem, *J. Volcanol. Geotherm. Res.*, *122*, 1–5, doi:10.1016/S0377-0273(02)00471-7.

J. Dufek, School of Earth and Atmospheric Sciences, Georgia Institute of Technology, 311 Ferst Drive, Atlanta, GA 30332, USA. (dufek@berkeley.edu)

M. Manga, Department of Earth and Planetary Science, University of California Berkeley, 307 McCone Hall, Berkeley, CA 94720, USA.